Advances in Nanochemistry

Article

Sensitization of copper oxide nanoparticles by Victoria Blue R for dye-sensitized solar cells: A DFT study

Received 20th November 2018,
Accepted 27th November 2018,
DOI:10.22126/anc.2019.3402.1007

Farimah Mousavi*, Avat Arman Taherpour*

Faculty of Chemistry, Razi University, Kermanshah, 67149-67346, Iran

Abstract

The model structures of the copper oxide (CuO) nanoparticles and the Victoria blue R (VBR) dye were drawn and optimized using density functional theory (DFT) methods. The orbital energy diagrams of CuO, VBR, and the VBR-sensitized CuO were calculated by means of DFT/B3LYP/6-31G* method. The study revealed the energy of the highest occupied molecular orbital (E_{HOMO}), the lowest unoccupied molecular orbital (E_{LUMO}), and the band gap ($\Delta E_{HOMO-LUMO}$) of the VBR molecule as -3.85, -2.77, and 1.08 eV, respectively. Same calculations on the model structure of CuO nanoparticles represented the band gap of 2.78 eV, which was decreased into 0.80 eV for the VBR-sensitized CuO. The ultraviolet-visible (UV-Vis), infrared (IR), and nuclear magnetic resonance (NMR) spectrums, as well as the effect of solvation on the molecular orbitals of the VBR molecule, were also calculated. The UV-Visible spectra of the dye display two broad absorption peaks in the visible region. In addition, the electrostatic potential and the local ionization potential maps of the modeled VBR-sensitized CuO photoanode were illustrated and discussed. This study successfully describes the potential of VBR-sensitized CuO to be used as a photoanode in dye-sensitized solar cells (DSCs).

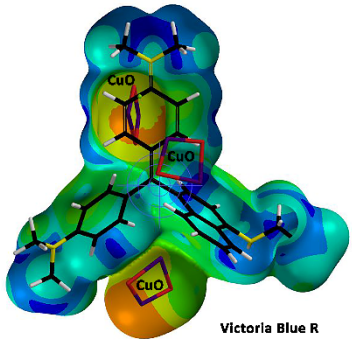

Keywords: *Dye-sensitized solar cell (DSC), Copper oxide nanoparticles, Victoria blue R (VBR), Density functional theory (DFT).*

Introduction

Dye-sensitized solar cells (DSCs) are photoelectrochemical cells consist of three main elements: a mesoporous sensitized photoanode, a counter electrode, and a redox electrolyte.[1, 2] This type of third-generation solar cells have been fabricated through very cost-effective procedures and offers interesting properties that fulfill the market needs.[3] In a DSC, each element own some unique applicability which urges to encompass specific features and also to match with the features of other elements, operating the DSC device with potentially highest efficiency. The photoanode in DSCs is usually a wide bandgap crystalline mesoporous metal oxide nanomaterial.[1, 4] Various metal oxide nanomaterials (e.g. TiO_2, ZnO, SnO_2, etc.) have used in DSCs.[5] Although they contain significant effective-surface-area, owning the wide bandgap results in capturing the sunlight only in ultraviolet (UV) region, and not in the visible (Vis) or near-infrared (NIR) ones.[5] However, these two last regions of electromagnetic spectrum comprise a large portion of the solar spectrum received to the earth surface.[6] Therefore, sensitizing the mesoporous metal oxide with a low bandgap and broad absorption spectrum (especially in the visible region) is crucial. Furthermore, the charge separation process occurs through the injection of photoelectron from the excited dye into the conduction band (CB) of the semiconductor.[4] This leads to the creation of holes at the highest occupied molecular orbital (HOMO) of the dye. The oxidized dye would further be regenerated through the redox reaction of the redox couple (e.g. I^-/I_3^-).[5] Briefly, the oxidation of the redox couple takes places at the interface of photoanode/electrolyte, however, their reduction occurs at the interface of the counter electrode/electrolyte.[5] To this purpose, different redox couples like I^-/I_3^-, cobalt-based systems (Co^{2+}/Co^{3+}), $SCN^-/(SCN)_3^-$, Br^-/Br_3^- and $SeCN^-/(SeCN)_3^-$, ferrocene, etc. were employed in DSCs.[5, 7-10] A list of alternative redox systems for DSCs could be found in the work of Nusbaumer.[11]

Generally, a driving force is required for the DSC operation which is carried out by the difference in the electronic levels (or reduction potential) of the semiconductor and the dye molecule.[4] To this purpose, the bandgap of the dye must be shorter than the bandgap of the semiconductor and the lowest occupied molecular orbital (LUMO) of the dye must be higher than the conduction band (CB) of the semiconductor. It is also crucial that the oxidation potential value of the dye be more positive than the corresponding amount for the redox couple.

A group of the most common and efficient sensitizing agents is based on ruthenium-containing metalorganic dyes which adsorbed on TiO_2 nanostructures.[12, 13] These common sensitizers, e.g. N3, N719, and other similar dyes are able to provide the spatial separation of the LUMO and the HOMO, obtaining faster injection compared to recombination.[13-15] However, the harsh conditions of synthesizing the ruthenium-based dyes, their purification issues, and the inadequate availability of ruthenium complexes obviously restrict their application in DSCs.[4, 16] On the other side, the organic dyes contain the benefits of high molar extinction coefficient, low amount of used dye, a thinner semiconductor layer, smaller dark current, higher open-circuit potential (V_{oc}), the ability to tune the absorption wavelength, being environmentally-friendly, cost-effective price, and the relatively simple synthetic process.[4, 16-20]

Corresponding authors:
Farimah Mousavi, Email: farimah.mousavi@hotmail.com, and
Avat Arman Taherpour, Email: avatarman.taherpour@gmail.com

To the date, various natural and synthetic dyes have been used as sensitizers in DSCs. There are reports on employing natural dyes such as chlorophyll, pomegranate juice, betalain (from red beetroots), coumarin, indoline, and merocyanine as sensitizing dyes.[14, 21-25] Comprehensive discussions on the role of natural dyes in DSCs could be found in the work of Zhou et al.[26] and Richhariyaa et al.[27]

In order to choose or prepare a convenient compound for sensitizing the metal oxide semiconductor, there must be a suitable conjunction between the electronic levels of the sensitizing compound (e.g. dye) and the semiconductor. Constructing various DSC devices to find the favorable efficiency employing various materials and arrangements, costs a lot, however, by means of computational methods each material could be characteristically evaluated both solitude and in contact with other cell materials to find the best choice on assembling the efficient solar cell.[28] The relatively cheap and accurate density functional theory (DFT) method is convenient to investigate the optical and the band structure properties of different compounds. DFT is able to calculate a wide range of molecular properties which provides a satisfying relationship between the theoretical and the experimental results. This can also result in defining valuable guidelines for the geometric, electronic, and spectroscopic features of the under-study systems. These statements may declare that DFT is convenient to investigate the structure and the energy levels of non-bonded dye-sensitized photoanode.

In this study, by means of DFT calculations, we geometrically optimized the models of the dye Victoria blue R (VBR), the copper oxide nanoparticles (CuO), and the VBR-sensitized CuO photoanode as well as calculating their band structures. To the best of our knowledge, there is no published report on the application of VBR-sensitized CuO nanoparticles as photoanodes in dye-sensitized solar cells.

Computational calculation

All computational calculations were performed using Wavefunction Spartan 16' package.[29] The geometrical optimization and the molecular orbital energies of VBR, CuO, and VBR-sensitized CuO models were achieved by the DFT study using Becke (three-parameter)-Lee-Yang-Parr (functional) (B3LYP) and 6-31G* basis set.

Results and discussion

The optimized structure of the dye Victoria blue R

Figure 1 represents the geometrically optimized model structure of Victoria blue R with the label of atom number. The labels would be further useful in discussing the calculated spectrums. The dye has the molecular formula of $[C_{29}H_{32}N_3]Cl$ and the molecular weight of 458.049 amu.

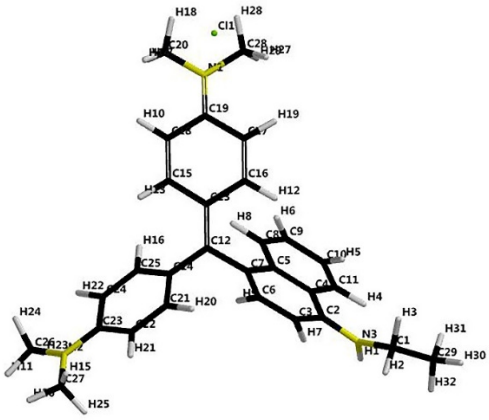

Figure 1. *The geometrically optimized Victoria blue R labeled with the atom numbers.*

The effect of solvation on the molecular orbital energy levels

The DFT study was performed to geometrically optimize the VBR model structure and also declare its band structures. As can be seen in Figure 2, the energy of the HOMO (E_{HOMO}), the LUMO (E_{LUMO}), and the HOMO-LUMO bandgap ($\Delta E_{HOMO-LUMO}$) of the VBR in vacuum condition are respectively calculated as -2.77, -3.85, and 1.08 eV. In order to evaluate the effect of solvation on the energy diagram of the VBR dye, the single point DFT calculation was applied in vacuum and five different solvents. According to the results in Figure 3, one may understand that the solvation has a huge impact on bandgap widening of VBR. However, no significant difference is observed among the calculated bandgap of VBR in different solvents consist of water, ethanol, acetone, dimethyl sulfoxide (DMSO), and dimethylformamide (DMF).

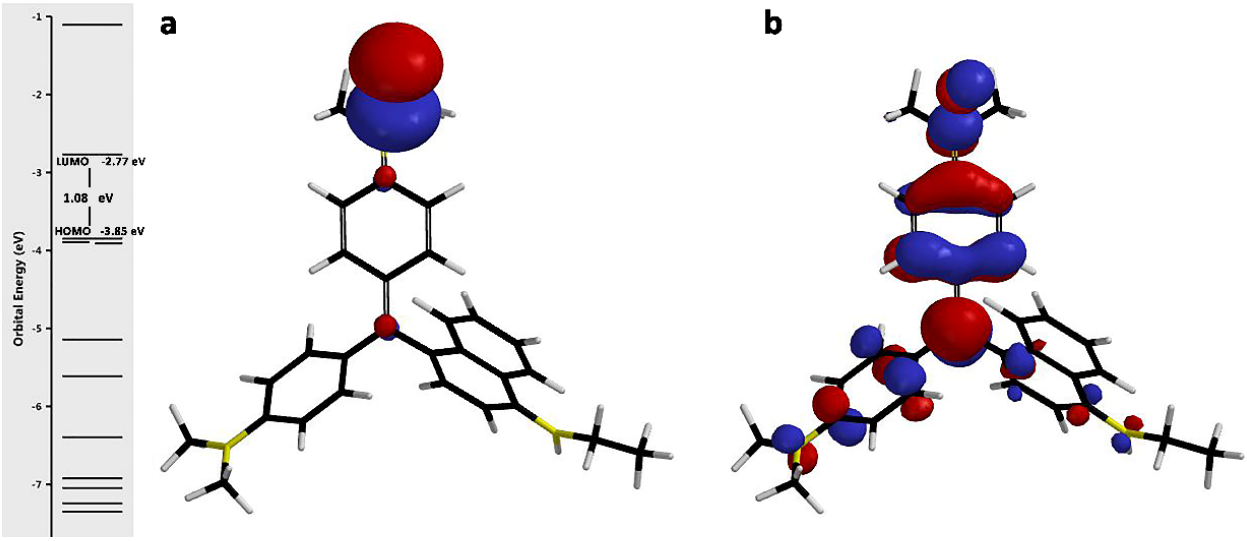

Figure 2. *The energy diagram and the a) HOMO and b) LUMO surfaces of Victoria blue R.*

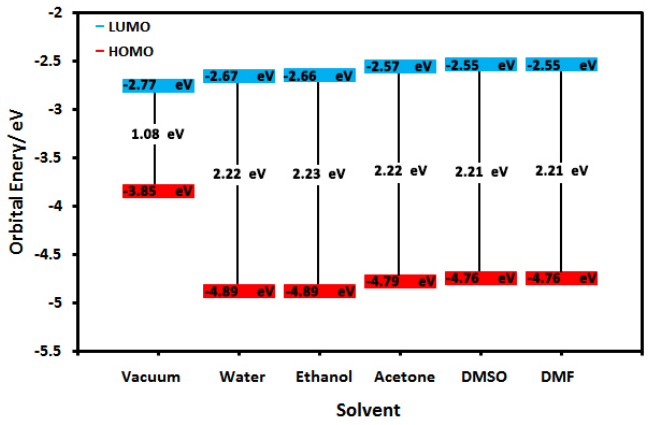

Figure 3. *The effect of solvation on the molecular orbital energy diagram of Victoria blue R.*

The spectroscopy of the dye Victoria blue R

The calculated UV-Vis, IR, nuclear magnetic resonance (^{1}H NMR and ^{13}C NMR) spectrums of the dye Victoria blue R were obtained using the single point DFT/B3LYP/6-31G* method. The calculated UV-Vis spectrum of Victoria blue R (Figure 4a) represents a broad spectrum from 430 to 700 nm with two absorption peaks at 521.63 and 622.97 nm which perfectly matches with the experimental absorption spectrum in published reports.[30] This makes the dye molecule highly suitable to be used as a sensitizer in dye-sensitized solar cells by broadening the absorbing light spectrum of the wide bandgap semiconductors (e.g. CuO).

Figure 4b displays the calculated IR spectrum of Victoria blue R. The obtained IR peaks, from long to short wavenumbers, are related to stretching vibration of the bond N3-H1 (3653 cm^{-1}), stretching vibration of C11-H4 (3395 cm^{-1}), asymmetric stretching vibration of C28-H27 with C28-H28, C28-H29 (3359 cm^{-1}), asymmetric stretching vibration of C29-H30 with C29-H31, C29-H32 (3332 cm^{-1}), asymmetric stretching vibration of C18-H10 with C15-H13 (3314 cm^{-1}), asymmetric stretching vibration of C28-H28 with C28-H27, C28-H29, and C20-18 with C20-H14, C20-H17 (3269 cm^{-1}), asymmetric stretching vibration of C26-H23 with C26-H11, C26-H24, and symmetric stretching vibration of C24-H22 with C24-H16 (3254 cm^{-1}), asymmetric stretching vibration of C25-H16 with C24-H22, C22-H21(3242 cm^{-1}), asymmetric stretching vibration of C22-H21 with C21-H20, C25-H16 (3235 cm^{-1}), asymmetric stretching vibration of C10-H5 with C9-H6, C11-H4 (3225 cm^{-1}), asymmetric stretching vibration of C6-H9 with C3-H7 (3207 cm^{-1}), asymmetric stretching vibration of C24-H22 with C25-H16 (3206 cm^{-1}), asymmetric stretching vibration of C21-H20 with C22-H21 (3186 cm^{-1}), asymmetric stretching vibration of C20-H14 with C20-H17, C20-H18, and C1-H3 with C1-H2 (3149 cm^{-1}), asymmetric stretching vibration of C9-H6 with C8-H8, C10-H5 (3145 cm^{-1}), asymmetric stretching vibration of C27-H15 with C27-H25, C27-H26 (3126 cm^{-1}), asymmetric stretching vibration of C28-H27 with C28-H28, C28-H29 (3119 cm^{-1}), symmetric stretching vibration of C1-H2 with C1-H3 (3104 cm^{-1}), asymmetric stretching vibration of C26-H11 with C26-H24, C26-H23 (3095 cm^{-1}), asymmetric stretching vibration of C17-H19 with C16-H12 (3093 cm^{-1}), asymmetric stretching vibration of C29-H32 with C29-H30, C29-H3 (3084 cm^{-1}), asymmetric stretching vibration of C8-H8 with C9-H6 (3069 cm^{-1}), asymmetric stretching vibration of C20-H17 with C20-H14, C20-H18 (3047 cm^{-1}), symmetric stretching vibration of C26-H11 with C26-H24, C26-H23 (3030 cm^{-1}), asymmetric stretching vibration of C16-H12 with C17-H19 (3014 cm^{-1}), asymmetric stretching vibration of C27-H25 with C27-H26, C27-H15 (2975 cm^{-1}), asymmetric stretching vibration of C3-H7 with C6-H9 (2935 cm^{-1}), symmetric stretching vibration of C27-H25 with C27-H26, C27-H15 (2930 cm^{-1}), and asymmetric stretching vibration of C29-H30 with C29-H31, C29-32 (2853 cm^{-1}) obtained from DFT calculations on the VBR model structure.

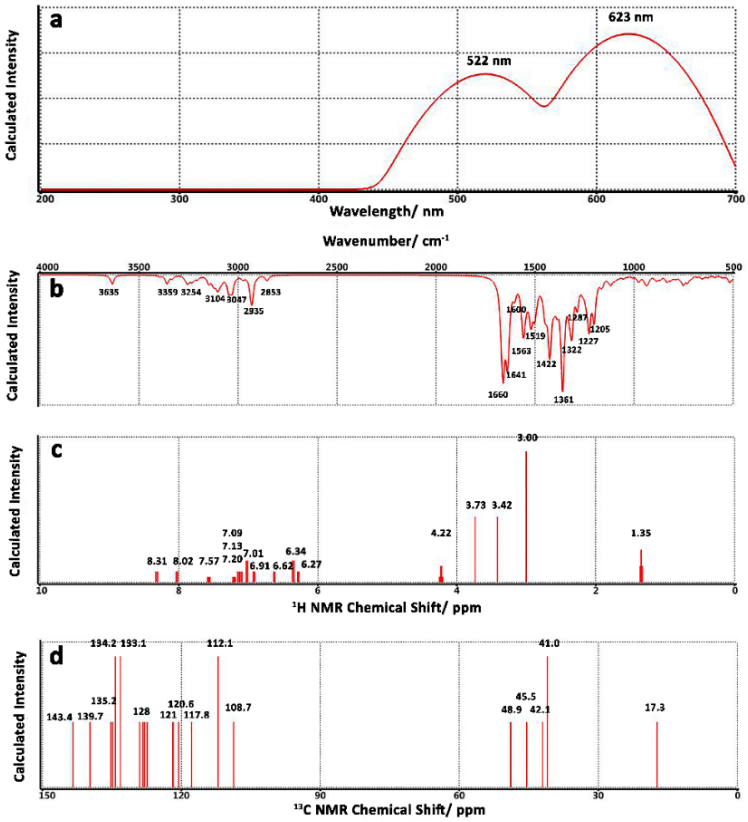

Figure 4. *The calculated a) UV-Vis, b) IR, c) ^{1}H NMR, and d) ^{13}C NMR spectrums of Victoria blue R (vacuum state, single molecule).*

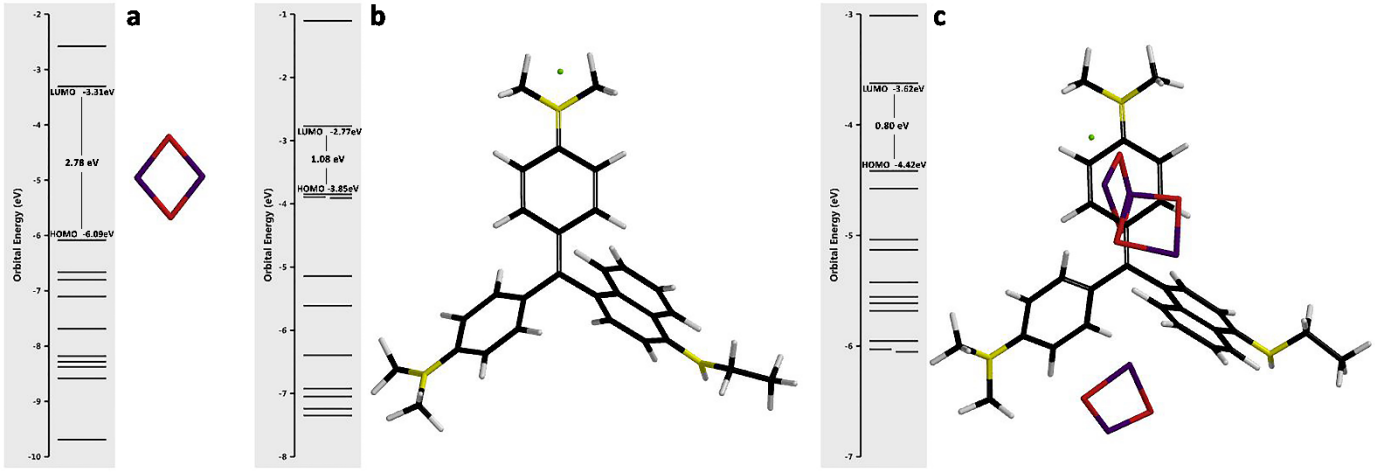

Figure 5. *The model structures and the moecular orbital diagrams of a) CuO nanoparticles, b) VBR, and c) VBR-sensitized CuO nanoparticles.*

Figure 4c and d represent the ^{1}H NMR and ^{13}C NMR of the VBR dye. In Figure 4c, the lines related to shifts in 1.35 ppm (H30, H31, H32), 3.00 ppm (H11, H23, H24, H15, H25, H26), 3.42 ppm (H14, H17, H18), 3.73 ppm (H27, H28, H29), 4.22 ppm (H2, H3), 6.27 ppm (H7), 6.34 ppm (H21, H22), 6.62 ppm (H9), 6.91 ppm (H10), 7.01 ppm (H16, H20), 7.09 ppm (H13), 7.13 ppm (H12, H19), 7.20 ppm (H5), 7.57 ppm (H6), 8.02 ppm (H8), and 8.31 ppm (H4) were obtained. Also, in Figure 4d the shifts at 17.3 ppm (C29), 41.0 ppm (C26, C27), 42.1 ppm (C1), 45.5 ppm (C20), 48.9 ppm (C28), 108.7 ppm (C3), 112.1 ppm (C22, C24), 117.8 ppm (C18), 120.6 ppm (C4), 121.7 ppm (C17), 121.8 ppm (C11), 121.9 ppm (C10), 127.4 ppm (C7), 128.0 ppm (C9), 128.3 ppm (C8), 129.0 ppm (C6), 133.1 ppm (C13, C14), 134.2 ppm (C21, C25), 134.8 ppm (C15), 135.2 ppm (C5), 139.7 ppm (C16), and 143.4 ppm (C2) were detected.

Sensitization of CuO nanoparticles with Victoria blue R

A structure consists of three CuO nanoparticles and one VBR molecule was modeled and optimized using DFT/B3LYP/6-31G* method. This study shows that the wide bandgap of CuO semiconductor (2.78 eV) shrinks into 0.8 eV, using the sensitization procedure with the VBR dye. This helps the resulting structure to capture the lights in the visible region rather than ultraviolet, and also prepare the root to the separation of the electron-hole pair (i.e. lower charge recombination) which is highly beneficial for different applications in dye-sensitized solar cells and photocatalytic reactions.

Table 1. *The calculated electronic levels of VBR, CuO, and VBR-sensitized CuO.*

N	Material	E_{HOMO} (eV)	E_{LUMO} (eV)	$\Delta E_{HOMO-LUMO}$ (eV)
1	CuO	-6.09	-3.31	2.78
2	VBR	-3.85	-2.77	1.08
3	VBR-sensitized CuO	-4.42	-3.62	0.80

Figure 6a and b respectively illustrate the electrostatic potential and the local ionization potential maps of the modeled VBR-sensitized CuO structure. The electrostatic potential maps (Figure 6a), also called electrostatic potential energy surfaces, display the three- dimensional (3-D) charge distributions of models which helps scientist to define the way different molecules interact with each other. These maps illustrate the variably charged areas of each molecule. It is known that the red and blue portions respectively indicate the lowest and the highest electrostatic potential energies and the intermediary colors belongs to the intermediary electrostatic potentials. There is the abundance of electrons in the areas with low potential (red color), however, those with high potential (blue color) are facing the relative absence of electrons. In the other word, the atoms with higher electronegativity would accordingly have the higher electron density around them compared to the other atoms. The chloride anion, as well as the oxygen atoms, are creating the areas with the lower potentials

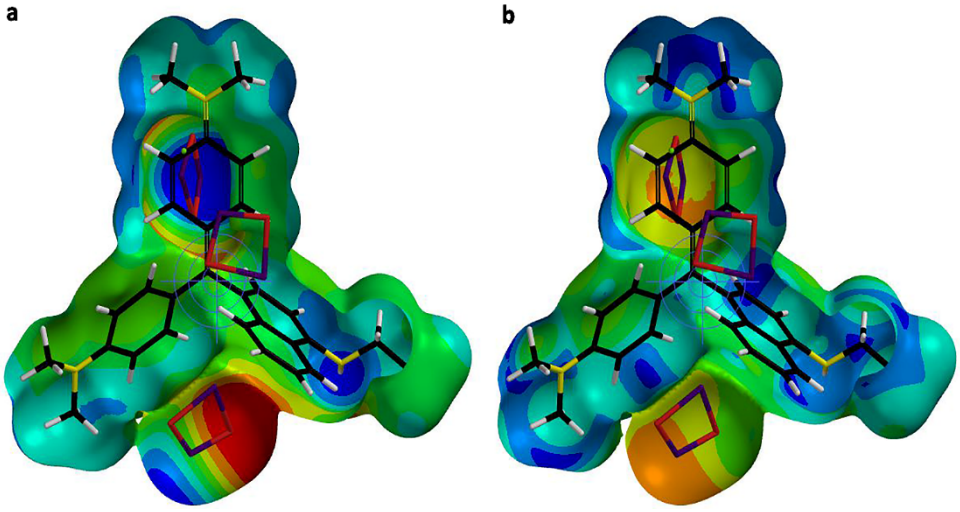

Figure 6. *a) The electrostatic potential and b) the local ionization potential maps of Victoria blue R.*

(red). However, the hydrogen and copper atoms are responsible for the blue colored areas with high electrostatic potentials.

As it is depicted in the local ionization potential map (Figure 6b), the copper atoms have the lowest ionization potential (red) among all atoms in the VBR-sensitized CuO model structure, while, the hydrogen atoms contain the highest ionization potentials (blue).

According to the results obtained in this study, the dye Victoria blue R can be suggested as a potentially favorable sensitizing agent, employing in dye-sensitized solar cells. The best matching metal oxide semiconductor to be sensitized with VBR was estimated in this study to be CuO nanoparticles.

Conclusion

The model structures of CuO nanoparticles, Victoria blue R dye, and the VBR-sensitized CuO were constructed and optimized using computational DFT method. The UV-Vis, IR, ^{1}H NMR, and ^{13}C NMR spectrums of the dye were calculated and discussed. The effect of solvation on the band structure of VBR was computationally evaluated by means of DFT study. The effect of solvation on the band structure of VBR was also evaluated. This study reveals that the VBR dye is a promising candidate to sensitize CuO nanoparticles which make the corresponding photoanode material potentially favorable to be used in dye-sensitized solar cells.

Aknowledgement

The authors would like to thank Razi University.

References

1. K. Hara and H. Arakawa, Handbook of Photovoltaic Science and Engineering, John Wiley & Sons, Ltd, (2005), Chichester, United Kingdom.
2. S. Ghasemi, S. R. Hosseini and F. Mousavi, *Colloid. Surface. A*, 520, **2017**, 477.
3. M. Grätzel, *J. Photoch. Photobio. C*, 4, **2003**, 145.
4. L. Ma and X. Zhan, Organic Optoelectronics, Wiley-VCH Verlag GmbH & Co. KGaA, (2013), Weinheim, Germany.
5. A. Hagfeldt, G. Boschloo, L. Sun, L. Kloo and H. Pettersson, *Chem. Rev.*, 110, **2010**, 6595.
6. K. Jäger, O. Isabella, A. H.M. Smets, R. A.C.M.M. van Swaaij and M. Zeman, Solar Energy; Fundamentals, Technology, and Systems, Delft University of Technology, (2014), Delft, Netherlands.
7. M. Freitag, F. Giordano, W. Yang, M. Pazoki, Y. Hao, B. Zietz, M. Grätzel, A. Hagfeldt and G. Boschloo, *J. Phys. Chem. C*, 120, **2016**, 9595.
8. T. Daeneke, A. J. Mozer, T.-H. Kwon, N. W. Duffy, A. B. Holmes, U. Bach and L. Spiccia, *Energ. Environ. Sci.*, 5, **2012**, 7090.
9. T. W. Hamann and J. W. Ondersma, *Energ. Environ. Sci.*, 4, **2011**, 370.
10. Z.-S. Wang, K. Sayama and H. Sugihara, *J. Phys. Chem. B*, 109, **2005**, 22449.
11. H. Nusbaumer, Doctoral (2004), EPFL.
12. M. K. Nazeeruddin, S. M. Zakeeruddin, R. Humphry-Baker, M. Jirousek, P. Liska, N. Vlachopoulos, V. Shklover, C.-H. Fischer and M. Grätzel, *Inorg. Chem.*, 38, **1999**, 6298.
13. Y. Huang, W.-C. Chen, X.-X. Zhang, R. Ghadari, X.-Q. Fang, T. Yu and F.-T. Kong, *J. Mater. Chem. C*, 6, **2018**, 9445.
14. D. Zhang, S. M. Lanier, J. A. Downing, J. L. Avent, J. Lum and J. L. McHale, *J. Photoch. and Photobio. A*, 195, **2008**, 72.
15. M. K. Nazeeruddin, A. Kay, I. Rodicio, R. Humphry-Baker, E. Mueller, P. Liska, N. Vlachopoulos and M. Graetzel, *J. Am. Chem. Soc.*, 115, **1993**, 6382.
16. D. Joly, L. Pellejà, S. Narbey, F. Oswald, J. Chiron, J. N. Clifford, E. Palomares and R. Demadrille, *Sci. Rep.*, 4, **2014**, 4033.
17. R. Li, J. Liu, N. Cai, M. Zhang and P. Wang, *J. Phys. Chem. B*, 114, **2010**, 4461.
18. Z. S. Wang, Y. Cui, K. Hara, Y. Dan-oh, C. Kasada and A. Shinpo, *Adv. Mater.*, 19, **2007**, 1138.
19. A. Mishra, M. K. Fischer and P. Bäuerle, *Angew Chem. Int. Edit.*, 48, **2009**, 2474.
20. M. Liang and J. Chen, *Chem. Soc. Rev.*, 42, **2013**, 3453.
21. A. Kay and M. Graetzel, *J. Phys. Chem.*, 97, **1993**, 6272.
22. U. Adithi, S. Thomas, V. Uma and N. Pradeep, *AIP Conf. Proc.*, 1512, **2013**, 208.
23. V. Saxena, P. Veerender, S. P. Koiry, A. K. Chauhan, D. K. Aswal, S. Mula, N. Shivran, S. Chattopadhyay and S. K. Gupta, *AIP Conf. Proc.*, 1451, **2012**, 272.
24. R. Hemmatzadeh and A. Mohammadi, *J. Theor. Appl. Phys.*, 7, **2013**, 1.
25. M. Thambidurai, N. Muthukumarasamy, D. Velauthapillai, N. Sabari Arul, S. Agilan and R. Balasundaraprabhu, *J. Mater. Sci. Mater. El.*, 22, **2011**, 1662.
26. H. Zhou, L. Wu, Y. Gao and T. Ma, *J. Photochem. Photobio. A*, 219, **2011**, 188.
27. G. Richhariya, A. Kumar, P. Tekasakul and B. Gupta, *Renew. Sustain. Energ. Rev.*, 69, **2017**, 705.
28. M. Oftadeh and L. Tavakolizadeh, *Int. Nano Lett.*, 3, **2013**, 1.
29. Wavefunction, Spartan '16-Quantum Mechanics Program, 2.0.0 edn., Wavefunction Inc., (2016), Irvine CA
30. M. Shamsipur, H. Reza Rajabi and O. Khani, *Mat. Sci. Semicon. Proc.*, 16, **2013**, 1154.